Influence of Side-Chain on Structural Order and Photophysical Properties in Thiophene Based Diketopyrrolopyrroles: A Systematic Study

4 AUTHORS, INCLUDING:

Mallari Naik

Manipal Technologies Ltd

12 PUBLICATIONS **128** CITATIONS

Venkatramaiah Nutalapati

University of Aveiro

**43** PUBLICATIONS **473** CITATIONS

Influence of Side-Chain on Structural Order and Photophysical Properties in Thiophene Based Diketopyrrolopyrroles: A Systematic Study

Mallari A. Naik, N. Venkatramaiah, Catherine Kanimozhi, and Satish Patil*

Solid State and Structural Chemistry Unit, Indian Institute of Science, Bangalore 560012, India

Ⓢ Supporting Information

ABSTRACT: In this work, we have synthesized a series of TDPP derivatives with different alkyl groups such as *n*-hexyl ($-C_6H_{13}$) **3a**, 2-ethylhexyl (-(2-$C_2H_5)C_6H_{12}$) **3b**, triethylene glycol mono methyl ether (-(CH$_2$CH$_2$O)$_{3c}$H$_3$, TEG) **3c**, and octadodecyl (-(8-$C_8H_{17})C_{12}H_{22}$) **3d**. *N,N* dialkylation of thiophene-diketopyrrolopyrrole (TDPP, **1**) strongly influences its solubility, solid state packing, and structural order. These materials allow us to explicitly study the influence of alkyl chain on solid state packing and photophysical properties. TDPP moiety containing two different alkyl groups **3e** (TEG and 2-ethylhexyl) and **3f** (TEG and *n*-hexyl) were synthesized for the first time. The absorption spectra of all derivatives exhibited a red shift in solid state when compared to their solution spectra. The type of alkyl chains leads to change in the optical band gaps in solid state. The fluorescence study reveals that TDPP derivatives have strong $\pi-\pi$ interaction in the solid state and the extent of bathochromic shift is due to combination of intramolecular interaction and formation of aggregates in solid state. This behavior strongly depends on the nature of alkyl chain. The presence of strong C–H···O inter chain interactions and CH–π interactions in solid state exhibits strong influence on the photophysical properties of TDPP chromophore.
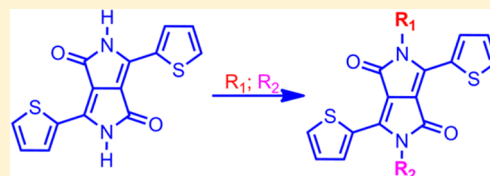
◼ INTRODUCTION

The major advantage of organic materials over conventional inorganic semiconductors is processability by common organic solvents. The solution processability has been achieved by covalently linking different alkyl chains to the backbone of the chromophore which renders it soluble. Recently, it has been found[1−3] that the alkyl chain of conjugated polymers immensely influences the photophysical and electronic properties and its device performance. In the past decade different types of low band gap conjugated polymers[4−11] have been synthesized by incorporating various alkyl chains for optoelectronic devices. Among them, diketopyrrolopyrrole (DPP) **1** and **2** (Figure 1) based conjugated copolymers have received great attention by many researchers.[12,13] These materials have been demonstrated to be potential donors due to their desirable properties such as broad optical absorption, chemical and thermal stability, and ease of synthesis and structural modifications by a variety of donating substituents.[12−14]
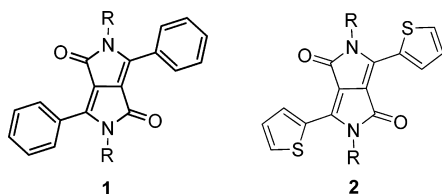

Figure 1. Phenyl (PDPP) and thiophene (TDPP) substituted DPP; *R* = alkyl or alkoxy chain.

Among the different types of DPP derivatives, 3,6-di-(thiophen-2-yl)pyrrolo[3,4-c]pyrrole-1,4 (2H,5H)-dione **2** (TDPP) based conjugated polymers has been extensively studied for bulk heterojunction (BHJ)[15−18] solar cells and organic field effect transistor (OFET).[19] The solubility of DPP derivatives in organic solvents is essential to fabricate thin film of these materials. As such, the DPP derivatives is insoluble in halogenated and other common organic solvents without *N,N* difunctionalization with alkyl chain; however, its solubility is reported in high polar solvents like DMSO, DMF, etc.[20] A major factor contributing to the insolubility of the DPP core is the strong intermolecular hydrogen-bonding between the lactam units. Thus, different alkyl groups have been substituted to achieve solubility in common organic solvents.[21−24] The major direction of research till today has been focused on the design of novel and highly soluble DPP based polymers by substituting various branched and linear alkyl chains.[25−28] However, the direct evidence for understanding the role of alkyl chains and its direct influence on the solid state photophysical behavior has not been explored. In this report, we have investigated the influence of alkyl chains on the TDPP unit and its structural variations on solid state properties such as molecular packing in single crystals, optical absorption, steady state and time-resolved emission, differential scanning calorimetry (DSC), and time dependent density functional theory (TDDFT) calculations. We have chosen different types of alkyl
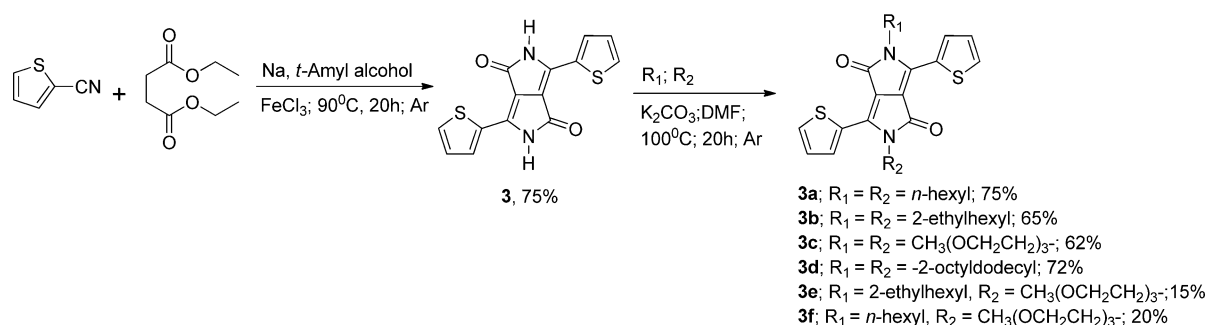
Scheme 1. Molecular Structures of Symmetrical (3a–d) and Unsymmetrical (3e,f) Alkylated TDPP
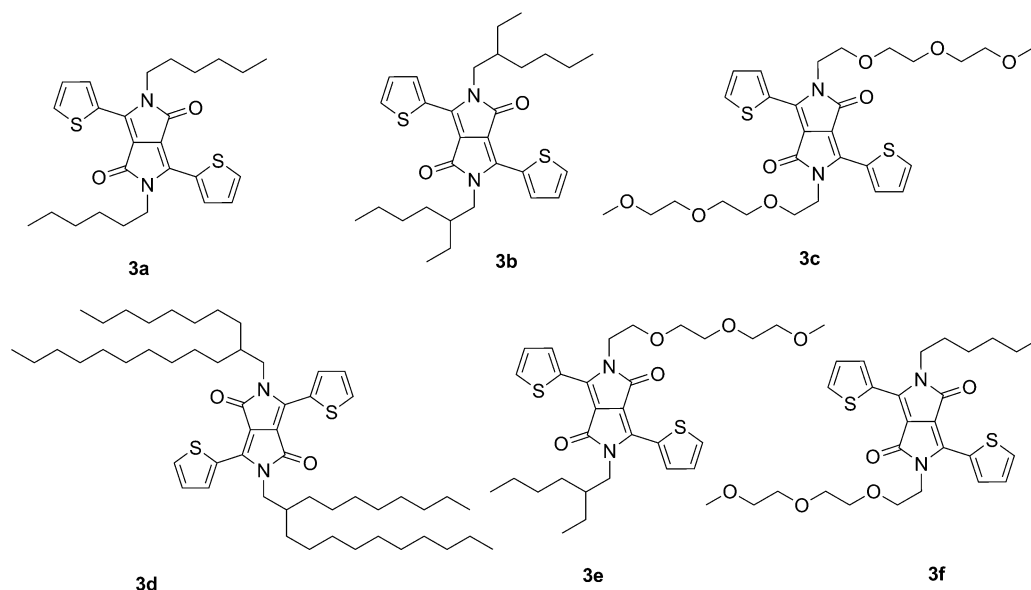
Scheme 2. Strategy for Synthesis of Different Alkyl Substituted TDPP

3, 75%

3a; $R_1 = R_2 = n$-hexyl; 75%
3b; $R_1 = R_2 = $ 2-ethylhexyl; 65%
3c; $R_1 = R_2 = CH_3(OCH_2CH_2)_3$-; 62%
3d; $R_1 = R_2 = $ -2-octyldodecyl; 72%
3e; $R_1 = $ 2-ethylhexyl, $R_2 = CH_3(OCH_2CH_2)_3$-; 15%
3f; $R_1 = n$-hexyl, $R_2 = CH_3(OCH_2CH_2)_3$-; 20%

chains by varying the nature of alkyl chains on TDPP core (Scheme 1). Symmetrical alkyl chain (n-hexyl, 2-ethylhexyl, TEG, and -$C_{20}H_{41}$) derivatives **3a–d** were synthesized according to previous procedures, and unsymmetrical alkyl chain derivative **3e** and **3f** were synthesized for the first time (Scheme 1). In the solid state, we observed several surprising trends in TDPP by systematically varying the alkyl chains. Single crystal X-ray analysis of these compounds are provided as an efficient platform to understand the structural effects at the molecular level. The alkyl substitution significantly affects the various photophysical properties. The n-hexyl chain substituted TDPP shows a larger bathochromic shift in the solid state as compared to other TDPP derivatives. This report provides guidelines to functionalize TDPP with a specific alkyl chain to render the solubility and achieve specific photophysical properties. Moreover, it also gives deeper insight into the role of the alkyl chain in determining the electronic properties of TDPP based conjugated materials.

■ EXPERIMENTAL SECTION

Materials. All reagents (AR grade) were purchased from S.D. Fine Chemicals, Spectrochem, Sigma-Aldrich and were used as received. All solvents for reactions were freshly distilled before use. All reactions were performed in oven-dried apparatus and were stirred magnetically.

Characterization. ^{1}H and ^{13}C NMR spectra were recorded on a Bruker 400 MHz (100 MHz ^{13}C) NMR spectrometer and

calibrated using TMS as an internal reference. Chemical shifts are reported in parts per million (ppm) and multiplicity is indicated using the following abbreviations: s (singlet), d (doublet), t (triplet), q (quartet), m (multiplet), sb (broad singlet), and db (broad doublet). The UV–visible spectra were recorded on a Perkin-Elmer (Lambda 35) UV–visible spectrometer. All of the spectra in solution were recorded in $CHCl_3$ (conc. One ×10^{-5} mol/L), and the spectra in the solid state were recorded from films of compounds spin coated on quartz substrate. Steady-state fluorescence emission studies were carried out with Spex FluoroLog-3 spectrofluorometer (Jobin-Yvon Inc.). Differential scanning calorimetry (DSC) was recorded on Mettler Toledo DSC1 STARe system (chiller cooled) with N_2 flow of 40 mL/min with an empty Al pan taken as standard. All samples were heated up to 10 °C above their melting point at a heating rate of 10 °C/min.

Single crystal X-ray diffraction data sets were collected on an Oxford Xcalibur (Mova) diffractometer[29] equipped with a EOS CCD detector using Mo Kα radiation (λ = 0.71073 Å). The crystal was maintained at the desired temperature during data collection using the Oxford instruments Cryojet-HT controller.[30] All structures were solved by direct methods using SHELXS-97 and refined against F2 using SHELXL-97.[31] H-atoms were fixed geometrically and refined isotropically. The WinGX package[32] was used for refinement and production of data tables, and ORTEP-3[33] for structure visualization and making molecular representations showing the ellipsoids at

30% probability level. Analysis of the H-bonded and $\pi-\pi$ interactions was carried out using PLATON[34] for all of the structures. Packing diagrams were generated by using MERCURY.[35] All quantum chemical calculations were carried out in the Gaussian 03 program by using the hybrid function B3LYP with 6-31g* basis set. After the optimization of the geometrical structures, TD-DFT calculations were performed at the B3LYP level with the 6-31g* basis set implemented in the Gaussian 03 program suite. The results were analyzed using Gauss View from Gaussian Inc.

Synthesis. The targeted molecules (**3a–d**) were synthesized according to the known procedure as described in literature.[36,37] The synthetic route and the molecular structures are illustrated in Scheme 2. The derivatives of TDPP Tosyl TEG ($CH_3(OC_2H_5)_3OTs$), as an alkylating agent, was initially synthesized by tosylating the triethylene glycol mono methyl ether (TEG, $CH_3(OC_2H_5)_3OH$) as from reported procedure.[38] The molecules **3e** and **3f** were synthesized by taking statistical equivalence both alkyl halide and tosyl TEG along with TDPP. All of the alkylated TDPP were characterized by ^{1}H NMR, ^{13}C NMR, and HRMS (ESI).

Synthesis for Compounds 3a−d. 3,6-di(thiophen-2-yl)-pyrrolo[3,4-c]pyrrole-1,4(2H,5H)-dione (TDPP) (0.5gm, 1.66 mmol) and potassium carbonate (0.81gm, 5.83 mmol) were taken in freshly distilled DMF (10 mL), stirred and heated at 120 °C for 1h. Corresponding alkyl halides/tosylated TEG (4.32 mmol) were dissolved in 10 mL of DMF was added dropwise for over 30 min. After complete dropwise addition the reaction was stirred and heated at 130 °C for 20h. The progress of the reaction was monitored by thin layer chromatography (TLC). On completion, DMF was removed under vacuum distillation. To the concentrated solution distilled water (200 mL) was added. The organic phases was extracted with CH_2Cl_2 (3 × 50 mL), washed with brine and dried over anhydrous $MgSO_4$. Crude mixture obtained was purified with silica gel chromatography eluting with hexane: ethyl acetate (9:1 to 7:3) in case of compounds **3a**, **3b** and **3d**. In case of **3c** the viscous purple liquid obtained was purified by silica gel chromatography, eluting with CH_2Cl_2/acetone (9:1 to 8:2) to give red solid.[38]

2,5-Dihexyl-3,6-di(thiophen-2-yl)pyrrolo[3,4-c]pyrrole-1,4-(2H,5H)-dione (3a). 75%: δ 8.93 (d, J = 3.9 Hz, 2H), 7.64 (d, J = 5.1 Hz, 2H), 7.29 (d, J = 4.9, 4.0 Hz, 2H), 4.12−4.01 (m, 4H), 1.80−1.69 (m, 4H), 1.48−1.37 (m, 4H), 1.36−1.26 (m, 8H), 0.88 (t, J = 7.0 Hz, 6H). ^{13}C NMR (101 MHz, CDCl₃)δ 161.38, 140.03, 135.22, 130.63, 129.80, 128.59, 107.73, 42.22, 31.40, 29.91, 26.53, 22.53, 13.98 ppm. HRMS (ESI-TOF) calculated for $C_{26}H_{32}N_2O_2S_2$ (M+Na)⁺: *m/z*: 491.18; found: 491.18

2,5-Bis(2-ethylhexyl)-3,6-di(thiophen-2-yl)pyrrolo[3,4-c]-pyrrole-1,4(2H,5H)-dione (3b). 65% ^{1}H NMR (400 MHz, CDCl₃)δ 8.89 (d, J = 3.7 Hz, 2H), 7.63 (d, J = 5.0 Hz, 2H), 7.28 (d, J = 4.3 Hz, 2H), 4.12 − 3.91 (m, 4H), 1.86 (d, J = 6.0 Hz, 2H), 1.49 − 1.08 (m, 16H), 0.87 (dd, J = 16.6, 7.3 Hz, 12H) ppm.^{13}C NMR (101 MHz, CDCl₃)δ 161.70, 140.37, 135.21, 130.46, 129.77, 128.36, 107.86, 45.79, 39.01, 30.13, 28.29, 23.47, 22.99, 13.96, 10.41 ppm. HRMS (ESI-TOF) calculated for$C_{30}H_{40}N_2O_2S_2$ (M+Na)⁺: *m/z*: 547.24; found: 547.24

2,5-Bis(2-(2-(2-methoxyethoxy)ethoxy)ethyl)-3,6-di-(thiophen-2-yl)pyrrolo[3,4-c]pyrrole-1,4 (2H, 5H)-dione (3c). 62% ^{1}H NMR (400 MHz, CDCl₃)δ 8.75 (d, J = 3.9 Hz, 2H), 7.64 (d,J = 5.1 Hz, 2H), 7.17 (d, J = 5.1 Hz, 2H), 4.29 (t, J = 6.3 Hz, 4H), 3.80 (t, J = 6 Hz, 2H), 3.65−3.47 (m, 16H), 3.34 (s, 6H) ppm. ^{13}C NMR (101 MHz, CDCl₃)δ 161.6, 140.5, 135.0, 131.1, 129.9, 128.6, 108.0, 72.1, 70.9, 70.7, 69.1, 59.2, 42.0 ppm. HRMS (ESI-TOF) calculated for$C_{28}H_{36}N_2O_8S_2$ (M+Na)⁺: *m/z*: 615.18; found 615.18

2,5-Bis(2-octyldodecyl)-3,6-di(thiophen-2-yl)pyrrolo[3,4-c]-pyrrole-1,4(2H,5H)-dione (3d). **3d** was synthesized according to the reported procedure[38] in 72% yield.^{1}H NMR (400 MHz, CDCl₃) δ 8.87 (d, J = 3.8 Hz, 2H), 7.62 (d, J = 5.0 Hz, 2H), 7.27 (d, J = 5.1 Hz, 2H), 4.02 (d, J = 7.6 Hz, 4H), 1.90 (s, 2H), 1.58 (s, 4H), 1.38−1.20 (m, 60H), 0.86 (q, J = 6.1 Hz, 12H) ppm.^{13}C NMR (101 MHz, CDCl₃) δ 162.16, 140.37, 135.15, 130.39, 129.78, 128.32, 127.12, 107.88, 46.15, 37.67, 31.85, 31.81, 31.11, 29.94, 29.58, 29.49, 29.43, 29.29, 29.23, 26.14, 22.62, 22.60, 14.06 ppm.HRMS (ESI-TOF) calculated for$C_{54}H_{88}N_2O_2S_2$(M+Na)⁺: *m/z*: 883.62; found 883.61

2-(2-Ethylhexyl)-5-(2-(2-(2-methoxyethoxy)ethoxy)ethyl)-3,6-di(thiophen-2-yl)pyrrolo[3,4-c] pyrrole-1,4(2H,5H)-dione (3e). 3,6-Di(thiophen-2-yl)pyrrolo[3,4-c]pyrrole-1,4(2H,5H)-dione (TDPP) (0.5 g, 1.66 mmol), tetra butyl ammonium bromide (0.026 g, 0.083 mmol), and potassium carbonate (0.81 g, 5.83 mmol) were taken in freshly distilled DMF (10 mL) and stirred at room temperature for 1 h. 2-(2-(2-Methoxyethoxy)-ethoxy)ethyl *p*-toluenesulfonate (0.53 g, 1.66 mmol) and 2-ethylhexyl bromide (0.32 g, 1.66 mmol) taken in 10 mL of DMF was added slowly dropwise for over 2 h. After the complete addition, the reaction was stirred at room temperature for 3 h further stirred at 90 °C for 20 h. The progress of the reaction was monitored by TLC. On completion, DMF was removed under vacuum distillation. To the concentrated solution distilled water was added (50 mL). The organic phases was extracted with CH_2Cl_2 (3 × 25 mL), washed with brine and dried over anhydrous $MgSO_4$. Dark red compound obtained was purified with silica gel chromatography eluting with hexane:ethylacetate (7:3) to give a dark red sticky solid (139 mg, 15%). ^{1}H NMR (400 MHz, CDCl₃) δ 8.84 (d, J = 3.3 Hz, 1H), 8.78 (d, J = 3.2 Hz, 1H), 7.62 (dd, J = 6.3, 5.4 Hz, 2H), 7.26 (t, J = 5.4 Hz, 2H), 4.28 (t, J = 6.3 Hz, 2H), 4.00 (t, J = 6.7 Hz, 2H), 3.79 (t, J = 6.3 Hz, 2H), 3.67−3.62 (m, 2H), 3.60−3.54 (m, 4H), 3.50−3.45 (m, 2H), 3.33 (s, 3H), 1.89−1.79 (m, J = 5.5 Hz, 1H), 1.39−1.20 (m, 9H), 0.88−0.81 (m, 6H) ppm. ^{13}C NMR (101 MHz, CDCl₃) δ 161.71, 161.41, 140.63, 140.07, 135.20, 134.75, 130.69, 130.60, 129.68, 129.65, 128.35, 107.98, 107.64, 71.83, 70.65, 70.47, 68.90, 58.93, 45.74, 41.77, 38.99, 34.23, 31.57, 30.22, 30.12, 29.62, 29.57, 28.25, 23.41, 23.00, 13.98, 10.41 ppm. HRMS (ESI-TOF) calculated for $C_{29}H_{38}N_2O_5S_2$ (M+Na)⁺: *m/z*: 581.21; found: *m/z* 581.32.

2-Hexyl-5-(2-(2-(2-methoxyethoxy)ethoxy)ethyl)-3,6-di-(thiophen-2-yl)pyrrolo[3,4-c]pyrrole-1,4 (2H,5H)-dione (3f). The synthetic procedure for **3f** was similar to that of **3e** except that *n*-hexyl bromide (0.32 g, 1.66 mmol) was used instead of 2-ethylhexyl bromide to give a dark red sticky solid (177 mg, 20%). ^{1}H NMR (400 MHz, CDCl₃) δ 8.90 (d, J = 3.9 Hz, 1H), 8.77 (d, J = 3.9 Hz, 1H), 7.64 (dd, J = 10.8, 5.0 Hz, 2H), 7.29 (t, J = 4.5 Hz, 2H), 4.29 (t, J = 6.2 Hz, 2H), 4.11−4.00 (m, 2H), 3.79 (t, J = 6.2 Hz, 2H), 3.68−3.62 (m, 2H), 3.58 (dd, J = 11.1, 5.2 Hz, 4H), 3.50−3.44 (m, 2H), 1.73 (dd, J = 15.5, 8.0 Hz, 2H), 1.31 (dd, J = 7.8, 4.4 Hz, 5H), 0.88 (t, J = 6.7 Hz, 4H) ppm. ^{13}C NMR (101 MHz, CDCl₃) δ 161.94, 161.86, 140.82, 140.54, 135.87, 135.22, 131.40, 131.20, 130.19, 129.13, 128.90, 108.63, 107.77, 72.36, 71.20, 71.01, 69.43, 59.49, 42.67, 42.32, 31.87, 30.37, 30.17, 27.01, 23.03, 14.51 ppm. HRMS (ESI-
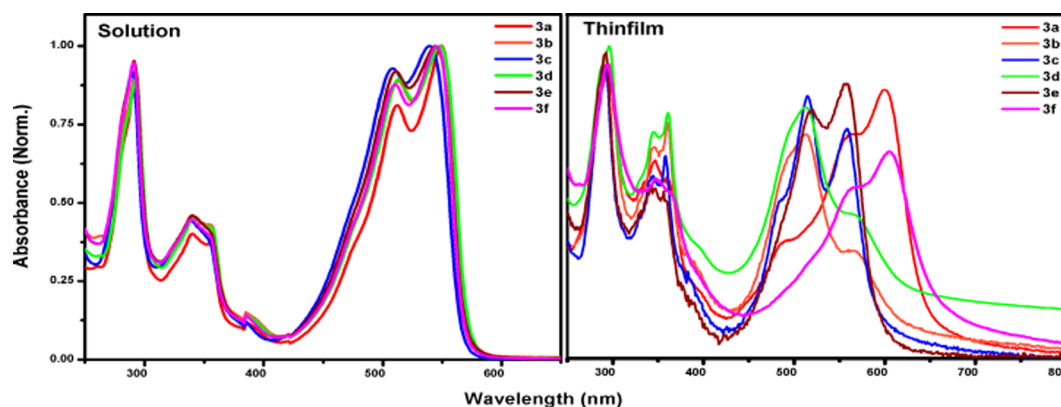
Figure 2. Absorption spectra of compounds **3a−f** taken in (a) solution and (b) thin film.
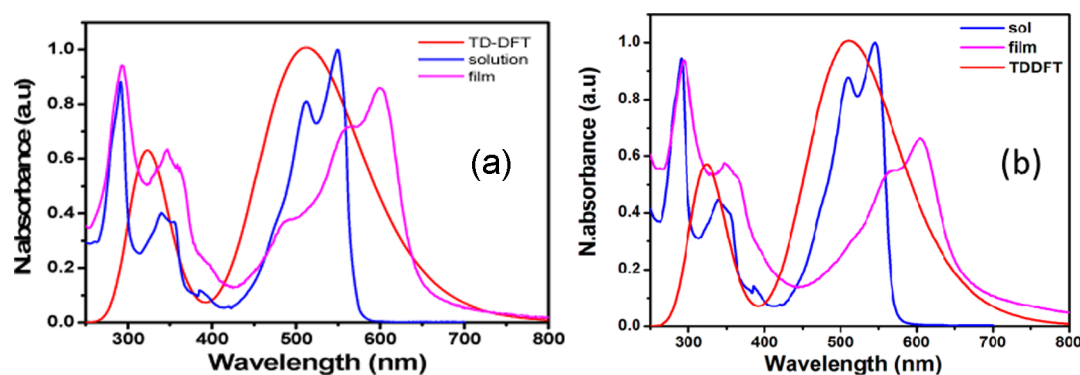

Figure 3. Comparison of UV−visible spectra between calculated and obtained spectra for compounds (a) **3a** and (b) **3f**.

TOF) calculated for $C_{27}H_{34}N_2O_5S_2$ (M+Na)$^+$: m/z: 553.19; found: m/z 553.41.

RESULTS

The synthesis of compounds **3a−d** was carried out according to a previously reported procedure.[39−41] Unsymmetrically alkylated compounds **3e** and **3f** were synthesized with slight modification from the reported procedures. After mixing thoroughly the base with TDPP in DMF, both the alkyl halides were taken together in a solution of DMF and added dropwise at room temperature with gradually increase the temperature to attain 90 °C. The formation of mono and dialkylated products was observed and was separated through column chromatography to get a moderate yield of **3e** and **3f**.

The optical absorption spectra of alkyl substituted TDPP (**3a−f**) obtained from both solution and the spin coated thin films are shown in the Figure 2. Thin films were prepared by spin coating 1 mg/mL CHCl₃ solutions on quartz substrates. The optical absorption spectra in chloroform exhibits three distinct absorption bands at ∼292 nm, which arises due to n → π* transitions, and the second absorption maximum is apparent in the range of ∼345−380 nm is due to π → π* transitions of diketopyrrolopyrrole moiety. Other strong absorption maxima with broad absorption spectra appear at ∼508 and ∼549 nm, respectively. These bands arise due to the intramolecular charge transfer (ICT) from thiophene (donor) moiety to DPP lactum unit. All the compounds exhibited a similar absorption pattern in solution with small variation in the absorption values that depends on type of alkyl chains on TDPP. This indicates that alkyl substitution on conjugated backbones of TDPP has much less impact on spectral shift in solution. The optical band gaps

calculated from absorption spectra lies in the range 2.02 ± 0.1 eV, and other significant optical properties are summarized in the ESI† Table S1. However, presence of different alkyl chains on TDPP shows large impact in solid state spectra (Figure 2b). All TDPP derivatives (**3a−3f**) exhibit bathochromic shift in thin film with broad absorption at longer wavelength region in comparison to solution spectra. The thin films of compounds **3b**, **3c**, **3d**, and **3e** showed red shifts of 12−17 nm, whereas **3a** and **3f** showed red shifts of 50 and 60 nm, respectively, in comparison to solution. The red shift in absorption maxima mainly arises due to strong intermolecular interactions and more planar conformation of the conjugated backbone. The more planar nature of the TDPP with linear alkyl chains favors formation of the aggregates in solid state and show enhanced red shift with a broader absorption pattern at longer wavelengths. The branched alkyl chains on **3b**, **3d**, and **3e** seems to significantly reduce the intermolecular interactions resulting in smaller red shift in comparison to **3a** and **3f** which have linear alkyl chains. The unsymmetrical alkylation in **3f** probably leads to larger red shift than symmetrical one **3a**. The optical band gaps of films are found to be lowered from 2.02 eV in solution to 1.77−1.98 eV in film. The appearance of strong red-shifted absorption of **3a** and **3f** in comparison to other compounds can be related to the backbone coplanarity which leads to improved molecular ordering and hence we observe red-shifted ICT band.

To further understand effect of alkyl chain substituents on absorption spectra and planarity of TDPP core TD-DFT calculations were performed. In all the derivatives **3a−f**, HOMO largely delocalized on thiophene ring and DPP core. The LUMO orbital largely distributed on the lactam ring for **3a**

D

dx.doi.org/10.1021/jp306365q | J. Phys. Chem. C XXXX, XXX, XXX−XXX

Table 1. Optical Band Gaps Calculated from the Absorption Spectra

|	state(s)	transitions	absorption (nm)	energy (eV)	oscillator strength (f)	dipole moment
3a	1	125 →126(58.66)	517.90	2.3940	0.4881	0.4904
	2	124 →126(67.18)	386.46	3.2082	0.0001	
		125 →127(16.17)				
3b	1	141 →142 (58.88)	516.04	2.4026	0.4881	0.3918
	2	140 →142 (66.8)	387.52	3.1994	0.0003	
		141 →143 (13.68)				
3c	1	157 →158 (58.68)	513.34	2.4153	0.5108	0.3316
	2	156 →158 (65.26)	377.45	3.2848	0.0000	
		157 →159 (23.39)				
3d	1	245 → 246(58.91)	519.84	2.3851	0.4667	0.3569
	2	244 → 246(67.63)	389.15	3.2848	0.0003	
		245 → 247(13.50)				
3e	1	149 →150 (58.93)	511.96	2.4218	0.4848	1.0540
	2	147 →150 (15.36)	382.38	3.2425	0.0022	
		148 →150 (65.57)				
		149 →151(16.63)				
3f	1	141 →142 (58.89)	511.48	2.4240	0.4841	1.5582
	2	140 →142 (66.62)	381.72	3.2481	0.0007	
		141 →143 (16.44)				
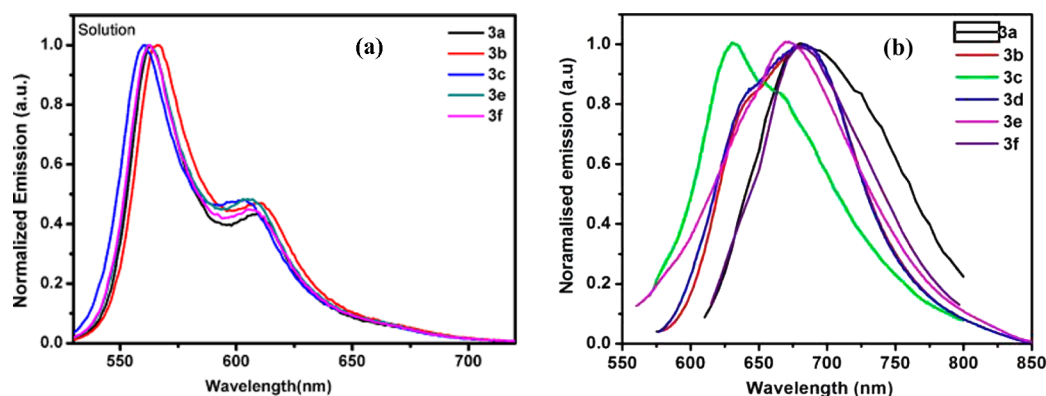
Figure 4. Emission spectra of compounds **3a–f** in (a) chloroform solution and (b) solid state.

(Figure S6, ESI[†]) whereas LUMO orbitals for other derivatives show (Figure S7−S11, ESI[†]) electron density on thiophene ring and DPP units due to orbital exchange interaction between HOMO-1 and LUMO. Calculated HOMO−LUMO gap was found to be in the range 2.44−2.49 eV and significant data is summarized in Table S1, ESI[†]. The highest band gap is observed for **3d** and lowest was for **3f**. These values were found to be nearly 0.3 to 0.35 eV higher than experimentally calculated values. This is related with various effects such as solvent effects and to variation in solid state to the gaseous states.

The optimized conformation shows that alkyl substituents influence the planarity of the TDPP unit to some extent. Lowest torsional angle observed for **3a** and **3f** are 1.914° and 1.146°, respectively, whereas bulkier alkyl chains **3b** and **3d** show a large β-torsional angle of ∼20° at one of the thiophene rings. The comparison of torsional angles between the optimized and the crystal structures of **3a−3c** revealed similar conformational changes upon optimization. The absorption spectra computed from the TD-DFT calculation is found to be nearly matching with solution spectra (Figure 3). Effect of torsional angle can possibly be ruled out in solution spectra due to free rotation in the bond connecting thiophene ring with DPP core. Observed differences in calculated and thin film

spectra is majorly due to the intermolecular interaction with minimal contribution from torsional angle.

All compounds exhibit good charge transfer transitions from HOMO → LUMO with similar oscillator strengths; $\pi \rightarrow \pi^*$ transitions were observed from the HOMO-1 → LUMO orbital (Table 1). For symmetrical alkyl chain substituents from **3a-d**, the dipole moment is found to be 0.3316−0.4881. The large dipole moment is observed for **3f** due to noncenter of symmetric alkyl chains. On a closer look at the energy levels of the HOMO and LUMO, **3f** has the lowest HOMO−LUMO gap followed by **3a**. Due to the strong red shift and electron-donating property of TEG chain affects the HOMO of **3f** than hexyl chains of **3a**. The energy difference between LUMO and LUMO+1 decreased with nature of N-terminal alkyl chain. This difference can be attributed to difference in orientation of thiophene units in either arm of the D-A-D systems.

The steady state emission spectra of TDPP alkyl derivatives are recorded in solution (chloroform) as well as in thin films. In solution, all compounds exhibit strong emissive nature and show small variation in emission wavelengths with respect to the nature of alkyl substituent. The solution emission spectra (Figure 4a) show two well resolved emission peaks at 560 and 610 nm with a Stoke's shift of ∼20 nm. Figure 4b shows thin film emission spectra of TDPP derivates, wherein a single
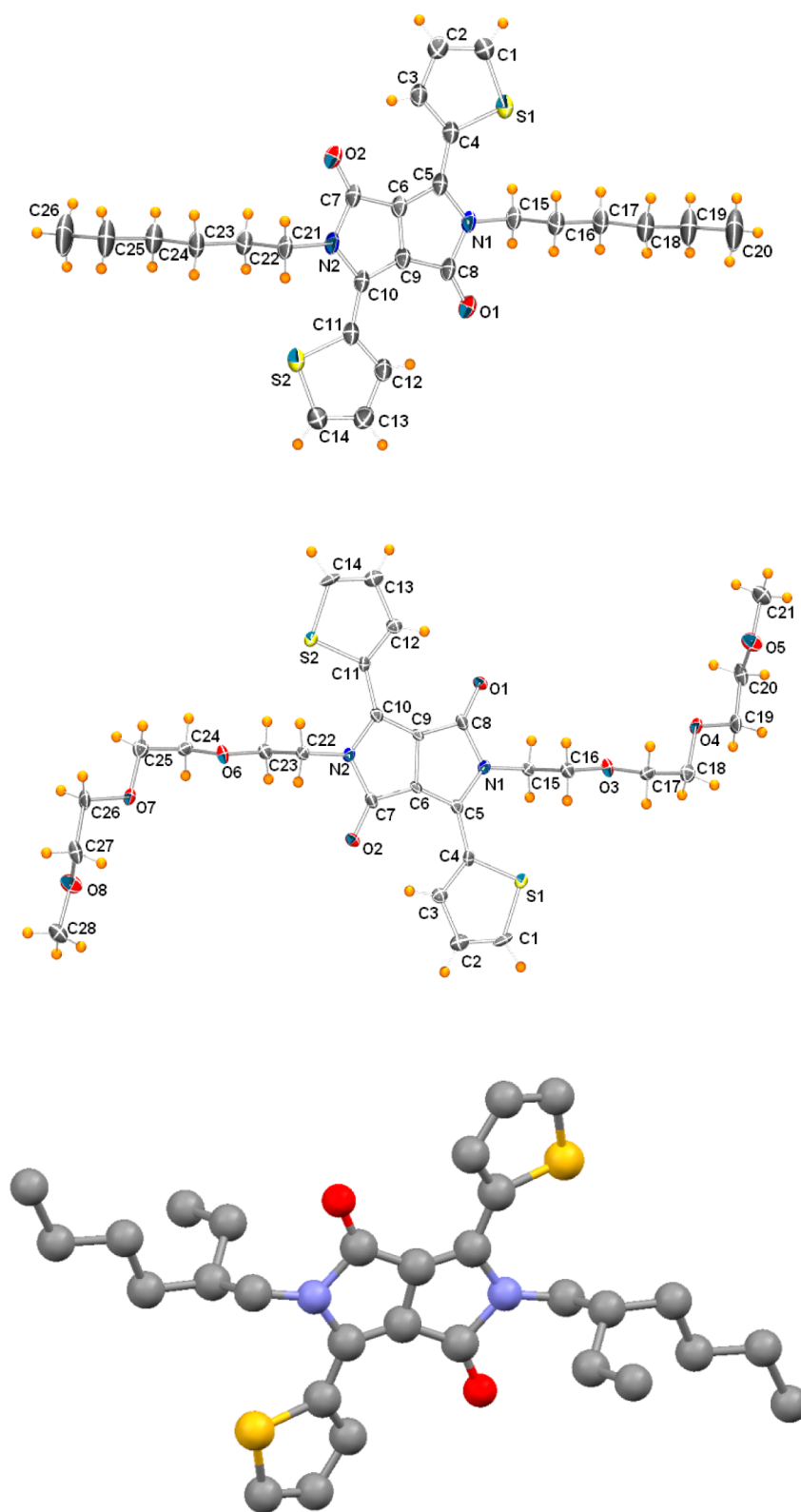
Figure 5. Single crystal XRD of compounds **3a−c**.

emission peak with full width at half-maximum (FWHM) of 60−105 nm was observed. The thin films exhibit a strong red shift in comparison to solution state, and data is summarized in Table S2. The extent red shift in emission wavelengths in thin film suggests that TDPP molecules will have strong intermolecular interaction and form aggregates in solid state

which state leads to appearance emission spectra at longer wavelength regions. The thin films show variation in Stoke's shift that strongly depends on the type of alkyl chain attached to the DPP unit. Compounds **3a**, **3c**, and **3f** having the linear alkyl chains on both sides show Stoke's shift in the range of 70−80 nm in solid state emission, whereas **3b**, **3d**, and **3e**

F

dx.doi.org/10.1021/jp306365q | *J. Phys. Chem. C* XXXX, XXX, XXX−XXX
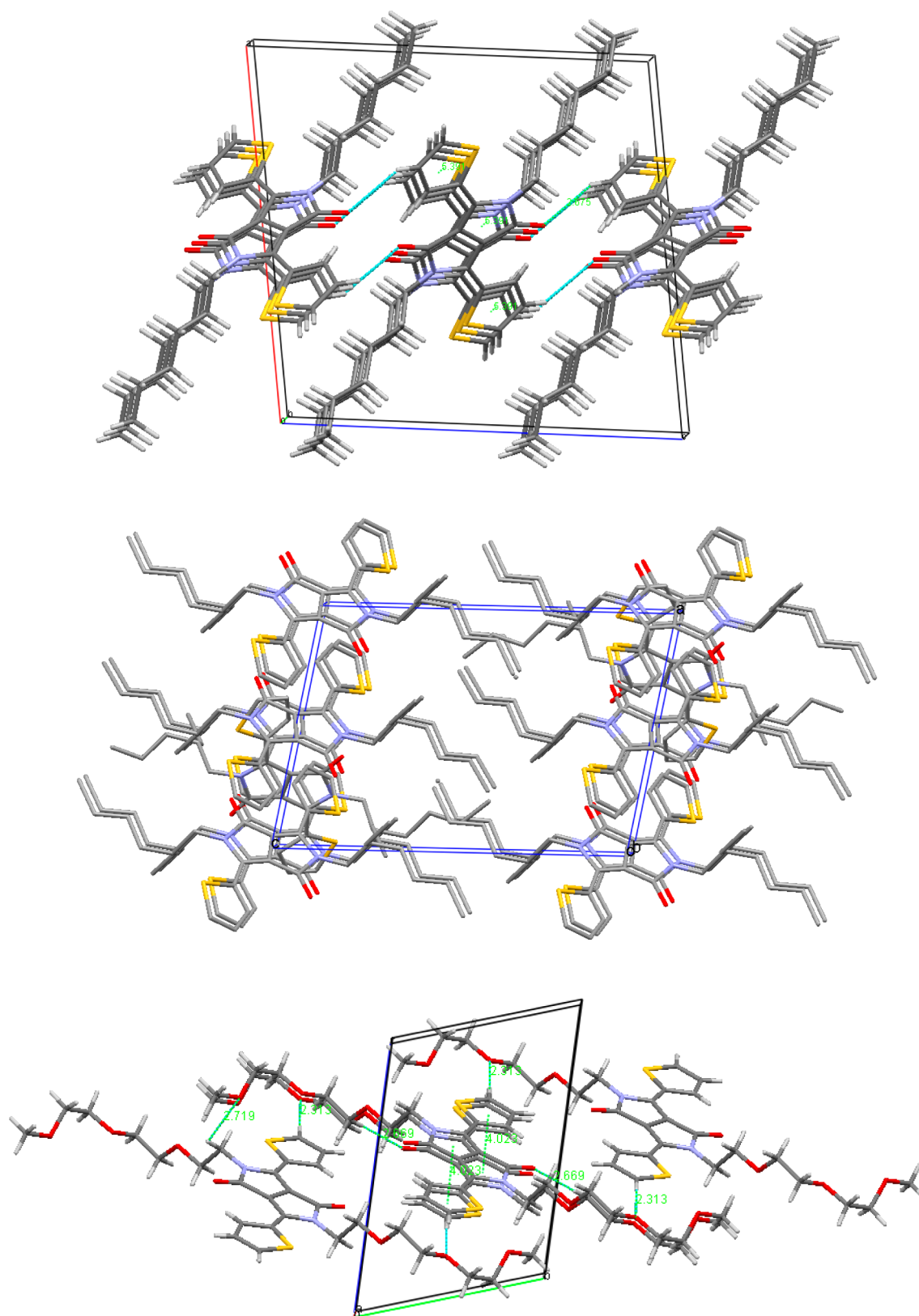
Figure 6. $\pi-\pi$ interactions in compounds **3a−c**.

having branched alkyl chains, at least on one side, showed a Stokes shift of 115−130 nm. The appearance of single broad emission in solid state arises due to the inherent nature of the alkyl chain with a rigid backbone, close packing of the

molecules, and well mixed electronic states as described in Table 1.

The solid state packing and molecular interactions were investigated by single crystal X-ray diffraction. **3a** and **3b** single crystals were grown from dichloromethane:methanol (8:2 v/v)

Table 2. Bond Length Data from Single Crystal X-ray Diffraction for Compounds 3a and 3c

	D−H···A	r(D−H)/Å	r(D−A)/Å	r(H···A)/Å	∠D−H···A/°	symmetry
3a	C3−H3···O1	0.924(0.032)	3.299(0.003)	2.675(0.031)	125.58 (2.51)	$x, -y + 1/2 + 1, +z + 1/2$
3b[a]						
3c	C(13)−H(13B)···O(1)	0.97	3.446(14)	2.60	147	$-x, 1 - y, -z$
	C−H Cg C(4)−H(4A)···Cg(1)	H···Cg 2.75	X···Cg (3.599(12)	X−H···Cg 147		symmetry $x, 1 + y, z$
	Cg(1)···Cg(3)	4.022(6)				$1 + x, y, z$

[a]Due to the glassy nature of the **3b**, the structure refinement was not comprehended.

solution, whereas **3c** single crystals were grown from dichloromethane:acetone (7:3 v/v) solution by slow evaporation of the solvents at room temperature. **3a−c** afforded in very thin cluster needle like crystals and compounds **3d−f** did not yield any good quality crystals. The single crystal XRD structures of **3a−c** are illustrated in Figure 5. The details of data collection and refinement are given in Figure 6, and selected bond lengths and angles are listed in Table 2. **3a** afforded in a monoclinic space group of $P21/c$ and the crystallographic center of symmetry is located at the midpoint of C6 and C9. The two thiophene rings are imposed in antiorientation with respect to each other and twisted by 6.37° relative to the mean plane of TDPP. The torsional angle between the thiophene units and the N-terminal hexyl chain is 10.05°, which indicates that thiophene rings are nearly coplanar to the TDPP unit. The crystal packing (Figure 6) shows that the molecule adopts weak intermolecular slipped $\pi-\pi$ stacking separated by distance of 3.614 Å. The molecules of adjacent $\pi-\pi$ stacks are engaged in supramolecular 1D networks running across the ac plane formed through intermolecular hydrogen bonding between C=O of the TDPP unit and the thiophene ring of the neighboring molecule by 2.675 Å (C−H···O). The crystal structure of **3b** revealed that it belongs to the triclinic space group $P\bar{1}$ with $Z = 4$. The arrangement of **3b** in the crystal is significantly different from that of **3a** as shown in Figure 6. The planar aromatic backbone and the type of alkyl chains are the important distinguishing features of the molecule. The molecules of adjacent $\pi-\pi$ stacks are engaged in the bc plane and the intermolecular hydrogen bonding observed between C=O of the TDPP unit and the terminal alkyl chain of the neighboring molecule through the C−H···O hydrogen bonding interaction with distances of 2.675 Å. The $\pi-\pi$ interaction is found to be 3.785 Å, which is slightly higher than **3a** indicating a weak $\pi-\pi$ interaction. The thiophene rings adjacent to the TDPP core are twisted by 6.64°, and the torsional angle is found to be 18.44. The increase in the torsional angle and increase in the $\pi-\pi$ distance are due to an increase in steric crowd at the second carbon of the alkyl chain. The protrusive nature of the side chains and the deviation in the planarity of thiophene rings lead to the improper overlaps of the aromatic molecular backbones.

To understand the effect of the hydrophilic alkyl chain on the N-terminal TDPP provoked our interest to introduce TEG chain on TDPP moiety. As shown in Figure 5, **3c** also crystallized in triclinic space group $P\bar{1}$ with $Z = 2$. The crystal packing shows that **3c** has a weak $\pi-\pi$ interaction of 4.021 Å, and the stacking arrangement is observed along the bc plane (Figure 6). The C−H···O intermolecular hydrogen bonding is similar to **3b** with a distance of 2.673 Å. In addition to the above, CH−π interactions exist at 2.851 Å and O−H interactions were observed between the oxygen atom of the side chain and the hydrogen atom of thiophene at 2.303 Å. The torsional angle is found to be smaller compare with the other

alkyl chains. This is due to the random oriented nature of the chain. From the above discussion, it is clearly understood that **3a** having stronger $\pi-\pi$ interactions than the other lead to tight packing with a rigid orientation. The steric hindrance created by the alkyl chain linked to the DPP ring could strongly affect the photophysical properties in the solid states.

Thermal behavior of these TDPP based compounds were studied by DSC. All of the compounds exhibited crystalline isotropic melting transitions and the melting transitions are summarized in Table 3 and are shown in Figure 7. From Table

Table 3. Variation of Melting Point of Different Compounds along with Their Molecular Weight

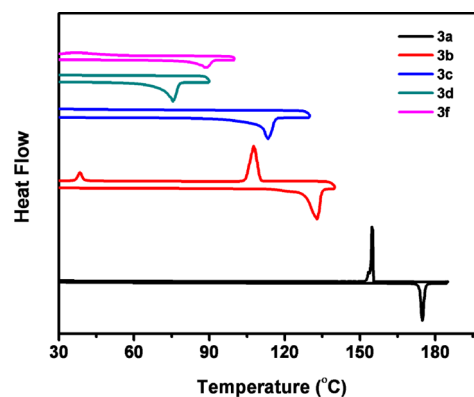| compound	melting point (°C)	mol. wt. (g/mol)
3a	174	468.67
3b	127	524.78
3c	120−122	592.72
3d	77−78	861.41
3e	semi solid	558.75
3f	83−85	530.69

Figure 7. DSC of all of the compounds recorded above their melting temperature.

3, it is interesting to observe that melting temperatures reduced drastically by changing the alkyl chain. This arises due to reduced intermolecular interactions among the TDPP cores which is a function of the alkyl chain. **3a** has got the linear hexyl chain melted at 176 °C, whereas **3b** and **3d** which have bulky branched alkyl chains melted around 127 and 77 °C, respectively. However this observation could not be generalized to compounds **3c** and **3f** which in-spite of having linear alkyl chains melted at lower temperatures in comparison to **3a**. This surprising behavior is obvious due to the TEG chains which due to the polarizable C−O bonds tend to be flexible thereby pushing the cores apart from each other. The same is also reflected in the cooling cycle of DSC where in both the **3c**, **3d**, and **3f** fail to crystallize.

DISCUSSION

The variation in absorbance spectra between solution and film can be explained on the basis of different alkyl chains, eventually leading to different intermolecular interactions. The evident red shift observed for compounds **3a** and **3f** in thin film spectrum leads us to conclude that intermolecular interactions should be a determining factor, which is influenced by the bulk of alkyl chains. Compounds **3a** and **3f** having linear chains attached to both their ends aids in efficient packing, leading to strong intermolecular interactions. In contrast, compounds **3b** and **3d** possessing the branched and bulkier alkyl chains lead to low red shift in film spectra. These results are further emphasized when we compare the shift obtained between solution and the film spectra. The highest red shift observed in **3f** could be due to noncovalent interactions among the TEG chains.[38] Unfortunately **3f** could not be crystallized which limits us to think on its $\pi-\pi$ stacking thoroughly. TD-DFT shows that the torsional angle between the thiophene ring and the DPP core is lowest for **3a** and **3f**, whereas it is highest for **3b** and **3d**. This shows the influence of alkyl chains on the planarity of the molecule. Bulky alkyl substituents induce rotation of the thiophene unit significantly and reduce the charge transfer integral between thiophene and central DPP core. As the planarity of the thiophene ring is disturbed, this effects not only the $\pi-\pi$ stacking but also the effective conjugation between the thiophene ring and the DPP core. Hence compounds **3a** and **3f** with a lower torsional angle show a better $\pi-\pi$ stacking/intermolecular interactions. However we find the effect of effective conjugation/intramolecular interactions to be minimal on photophysical studies.

SUMMARY AND OUTLOOK

In summary, we have synthesized TDPP units having different alkyl chains. TDPP units having two different alkyl chains have been reported for the first time. The solid state UV−visible spectra for all the molecules showed a red shift in comparison to their solution spectra; compounds **3a** and **3f** were significantly red-shifted. This indicated that packing played a significant role. Further investigation through TDDFT revealed that the alkyl chains played a pivotal role in determining the torsional angle between the central TDPP core and adjacent thiophene rings. The steady state emission spectra for all the compounds exhibit strong emissive nature and emission maxima varied slightly with nature of the alkyl substituent. The solid state packing and molecular interactions in **3a**, **3b**, and **3c** was investigated by single crystal X-ray diffraction. The X-ray data indicated the existence of the $\pi-\pi$ stacking. This study would give insights into choosing a particular alkyl chain, on the DPP core, specific for the desired application, rather than the existing random selection to achieve processability. Polymerization and device fabrication are a part of ongoing research and will be communicated in the due course of time.

ASSOCIATED CONTENT

Ⓢ Supporting Information

Methodology details, supplementary figures and other related information are available. This material is available free of charge via the Internet at http://pubs.acs.org.

AUTHOR INFORMATION

Corresponding Author
*Tel: +91-80-22932651. Fax: +91-80-23601310. E-mail: satish@sscu.iisc.ernet.in.

Notes
The authors declare no competing financial interest.

ACKNOWLEDGMENTS

REFERENCES

(1) Zhang, Y.; Kim, C.; Lin, J.; Nguyen, T.-Q. *Adv. Funct. Mater.* **2012**, *22*, 97−105.

(2) Walker, B.; Han, X.; Kim, C.; Sellinger, A.; Nguyen, T.-Q. *ACS Appl. Mater. Interfaces* **2012**, *4*, 244−250.

(3) Park, J. K.; Kim, C.; Walker, B.; Nguyen, T.-Q.; Seo, J. H. *RSC Adv.* **2012**, *2*, 2232−2234.

(4) Wu, J.-S.; Lin, C.-T.; Wang, C.-L.; Cheng, Y.-J.; Hsu, C.-S. *Chem. Mater.* **2012**, *24*, 2391−2399.

(5) Bijleveld, J. C.; Karsten, B. P.; Mathijssen, S. G. J.; Wienk, M. M.; de, L. D. M.; Janssen, R. A. J. *J. Mater. Chem.* **2011**, *21*, 1600−1606.

(6) Bijleveld, J. C.; Verstrijden, R. A. M.; Wienk, M. M.; Janssen, R. A. J. *J. Mater. Chem.* **2011**, *21*, 9224−9231.

(7) Cheng, Y.-J.; Wu, J.-S.; Shih, P.-I.; Chang, C.-Y.; Jwo, P.-C.; Kao, W.-S.; Hsu, C.-S. *Chem. Mater.* **2011**, *23*, 2361−2369.

(8) Min, J.; Peng, B.; Wen, Y.; Zhang, Z.-G.; Zhang, M.; Zhang, J.; Xie, Q.; Liu, Y.; Li, Y. *Synth. Met.* **2011**, *161*, 1832−1837.

(9) Sonar, P.; Singh, S. P.; Li, Y.; Ooi, Z.-E.; Ha, T.-j.; Wong, I.; Soh, M. S.; Dodabalapur, A. *Energy Environ. Sci.* **2011**, *4*, 2288−2296.

(10) Nielsen, C. B.; Ashraf, R. S.; Schroeder, B. C.; D'Angelo, P.; Watkins, S. E.; Song, K.; Anthopoulos, T. D.; McCulloch, I. *Chem. Commun.* **2012**, *48*, 5832−5834.

(11) Qian, G.; Qi, J.; Wang, Z. Y. *J. Mater. Chem.* **2012**, *22*, 12867−12873.

(12) Bürgi, L.; Turbiez, M.; Pfeiffer, R.; Bienewald, F.; Kirner, H.-J.; Winnewisser, C. *Adv. Mater.* **2008**, *20*, 2217−2224.

(13) Huo, L.; Hou, J.; Chen, H.-Y.; Zhang, S.; Jiang, Y.; Chen, T. L.; Yang, Y. *Macromolecules* **2009**, *42*, 6564−6571.

(14) Facchetti, A.; Marks, T. J.; Huang, H.; Chen, Z., Polyera Corporation, USA, WO2011119374A1, 2011.

(15) Bijleveld, J. C.; Zoombelt, A. P.; Mathijssen, S. G. J.; Wienk, M. M.; Turbiez, M.; de Leeuw, D. M.; Janssen, R. A. J. *J. Am. Chem. Soc.* **2009**, *131*, 16616−16617.

(16) Tamayo, A. B.; Dang, X.-D.; Walker, B.; Seo, J.; Kent, T.; Nguyen, T.-Q. *Appl. Phys. Lett.* **2009**, *94*, 103301.

(17) Zhou, E.; Yamakawa, S.; Tajima, K.; Yang, C.; Hashimoto, K. *Chem. Mater.* **2009**, *21*, 4055−4061.

(18) Loser, S.; Bruns, C. J.; Miyauchi, H.; Ortiz, R. P.; Facchetti, A.; Stupp, S. I.; Marks, T. J. *J. Am. Chem. Soc.* **2011**, *133*, 8142−8145.

(19) Qu, S.; Wu, W.; Hua, J.; Kong, C.; Long, Y.; Tian, H. *J. Phys. Chem. C* **2009**, *114*, 1343−1349.

(20) Zambounis, J. S.; Hao, Z.; Iqbal, A. *Nature* **1997**, *388*, 131−132.

(21) Zhu, S.; Dorh, N.; Zhang, J.; Vegesna, G.; Li, H.; Luo, F.-T.; Tiwari, A.; Liu, H. *J. Mater. Chem.* **2012**, *22*.

(22) Vala, M.; Weiter, M.; Vyňuchal, J.; Toman, P.; Luňák, S. *J. Fluoresc.* **2008**, *18*, 1181−1186.

(23) Weiter, M.; Salyk, O.; Bednář, P.; Vala, M.; Navrátil, J.; Zmeškal, O.; Vyňuchal, J.; Luňák, S., Jr. *Mater. Sci. Eng., B* **2009**, *165*, 148−152.

(24) Celik, S.; Ergun, Y.; Alp, S. *J. Fluoresc.* **2009**, *19*, 829−835.

(25) David, J.; Weiter, M.; Vala, M.; Vynuchal, J.; Kucerik, J. *Dyes Pigm.* **2011**, *89*, 137−143.

(26) Lee, J. S.; Son, S. K.; Song, S.; Kim, H.; Lee, D. R.; Kim, K.; Ko, M. J.; Choi, D. H.; Kim, B.; Cho, J. H. *Chem. Mater.* **2012**, *24*, 1316−1323.

(27) Li, Z.; Zhang, Y.; Tsang, S.-W.; Du, X.-M.; Zhou, J.-Y.; Tao, Y.; Ding, J.-F. *J. Phys. Chem. C* **2011**, *115*, 18002−18009.

(28) Vala, M.; Vynuchal, J.; Toman, P.; Weiter, M.; Lunak, S. *Dyes Pigm.* **2010**, *84*, 176−182.

(29) Oxford Diffraction(2009). CrysAlis PRO CCD and CrysAlis PRO RED. Oxford Diffraction Ltd; Yarnton, E.

(30) Oxford *Cryojet XL/HT controller*, Oxford Diffraction Ltd: Yarnton, England.

(31) Sheldrick, G. M. *Acta Crystallogr., Sect. A: Found. Crystallogr.* **2008**, *64*, 112−122.

(32) Farrugia, L. J. *J. Appl. Crystallogr.* **1999**, *32*, 837−838.

(33) Farrugia, L. *J. Appl. Crystallogr.* **1997**, *30*, 565.

(34) Spek, A. *J. Appl. Crystallogr.* **2003**, *36*, 7−13.

(35) Macrae, C. F.; Edgington, P. R.; McCabe, P.; Pidcock, E.; Shields, G. P.; Taylor, R.; Towler, M.; Streek, J. *J. Appl. Crystallogr.* **2006**, *39*, 453−457.

(36) Tamayo, A. B.; Tantiwiwat, M.; Walker, B.; Nguyen, T.-Q. *J. Phys. Chem. C* **2008**, *112*, 15543−15552.

(37) Kanimozhi, C.; Balraju, P.; Sharma, G. D.; Patil, S. *J. Phys. Chem. B* **2010**, *114*, 3095−3103.

(38) Mei, J.; Graham, K. R.; Stalder, R.; Tiwari, S. P.; Cheun, H.; Shim, J.; Yoshio, M.; Nuckolls, C.; Kippelen, B.; Castellano, R. K.; Reynolds, J. R. *Chem. Mater.* **2011**, *23*, 2285−2288.

(39) Turbiez, M. G. R.; Janssen, R. A. J.; Wienk, M. M.; Kirner, H. J.; Dueggeli, M.; Tieke, B.; Zhu, Y., Ciba Specialty Chemicals Holding Inc., Switz, WO2008000664A1, 2008.

(40) Wienk, M. M.; Turbiez, M.; Gilot, J.; Janssen, R. A. J. *Adv. Mater.* **2008**, *20*, 2556−2560.

(41) Cheng, Y.-J.; Yang, S.-H.; Hsu, C.-S. *Chem. Rev.* **2009**, *109*, 5868−5923.